Supporting Information

Table S1 Electrochemical three-electrode systems.

Electrochemical system (ECS)	Electrode layout	Working electrode	Electrolyte
Electrochemical system 1 (ECS1)	Three-electrode	$CoMoO_4$/NF or NF	40 mL 1 M KOH
Electrochemical system 2 (ECS2)	Three-electrode	$CoMoO_4$/NF or NF	40 mL 0.01 M QXL + 1 M KOH
Electrochemical system 3 (ECS3)	Three-electrode	$CoMoO_4$/NF	40 mL 0.01 M QXL + 1 M KOH + 0.01 M tert-butanol
Electrochemical system 4 (ECS4)	Three-electrode	$CoMoO_4$/NF or NF	200 mL 0.01 M QXL + 1 M KOH
Electrochemical system 5 (ECS5)	Three-electrode	$CoMoO_4$/NF or NF	40 mL 0.01 M THQXL + 1 M KOH
Electrochemical system 6 (ECS6)	Three-electrode	$CoMoO_4$/NF or NF	200 mL 0.01 M THQXL + 1 M KOH
Electrochemical system 7 (ECS7)	Three-electrode	GC	40 mL 0.01 M QXL + 1 M KOH
Electrochemical system 12 (ECS12)	Three-electrode	GF	40 mL 0.01 M QXL + 1 M KOH

Table S2 Electrochemical two-electrode systems in flow batteries.

Electrochemical system	Electrode layout	Positive electrode and its electrolyte	Negative electrode and its electrolyte
Electrochemical system 8 (ECS8)	Two-electrode in flow batteries	GF，40 mL 0.1 M $K_4[Fe(CN)_6]$ + 1 M KOH	$CoMoO_4$/NF，40 mL 0.01 M QXL + 1 M KOH
Electrochemical system 9 (ECS9)	Two-electrode in H-type batteries	GF，40 mL 0.1 M $K_4[Fe(CN)_6]$ + 1 M KOH	$CoMoO_4$/NF，40 mL 0.01 M QXL + 1 M KOH
Electrochemical system 10 (ECS10)	Two-electrode in H-type batteries	GF，40 mL 1 M KOH	$CoMoO_4$/NF，40 mL 1 M KOH
Electrochemical system 11 (ECS11)	Two-electrode in flow batteries	GF，40 mL 0.1 M $K_4[Fe(CN)_6]$	GF，40 mL 0.01 M QXL + 1 M KOH

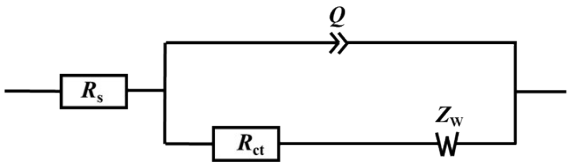

Fig. S1 EIS equivalent circuit diagram. R_s is the internal ohmic resistance, R_{ct} is the charge transfer impedance, Q is the phase angle element, and Z_w is the Warburg impedance.

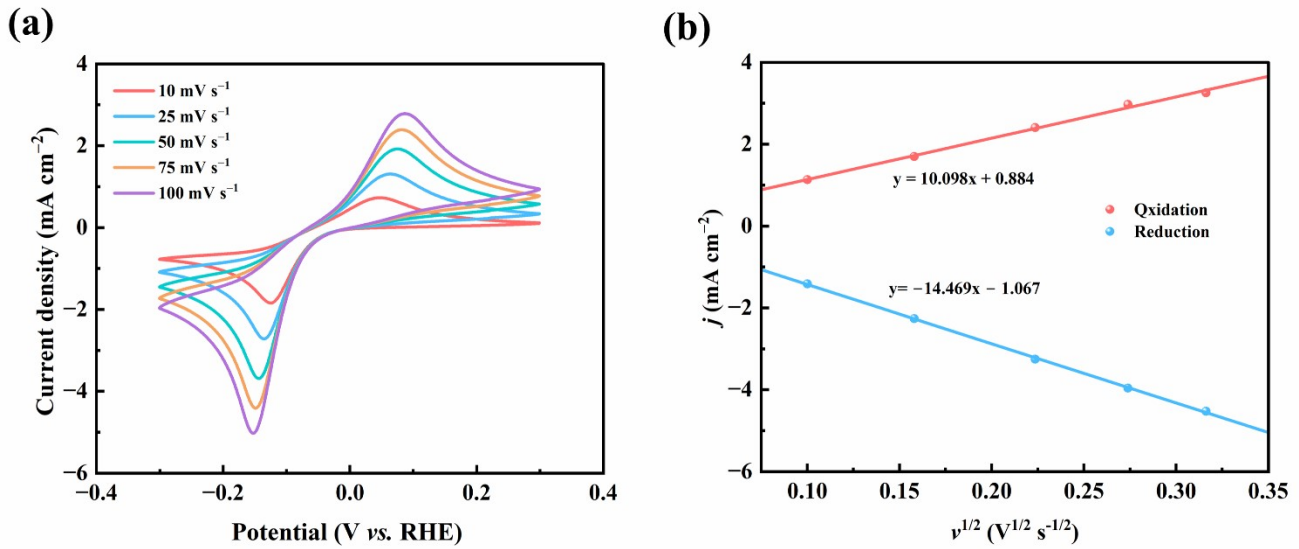

Fig. S2 (a) CV curves at different scan rates and (b) corresponding I_p–$v^{0.5}$ curves of the glassy carbon electrode (diameter of 3 mm) in ECS7.

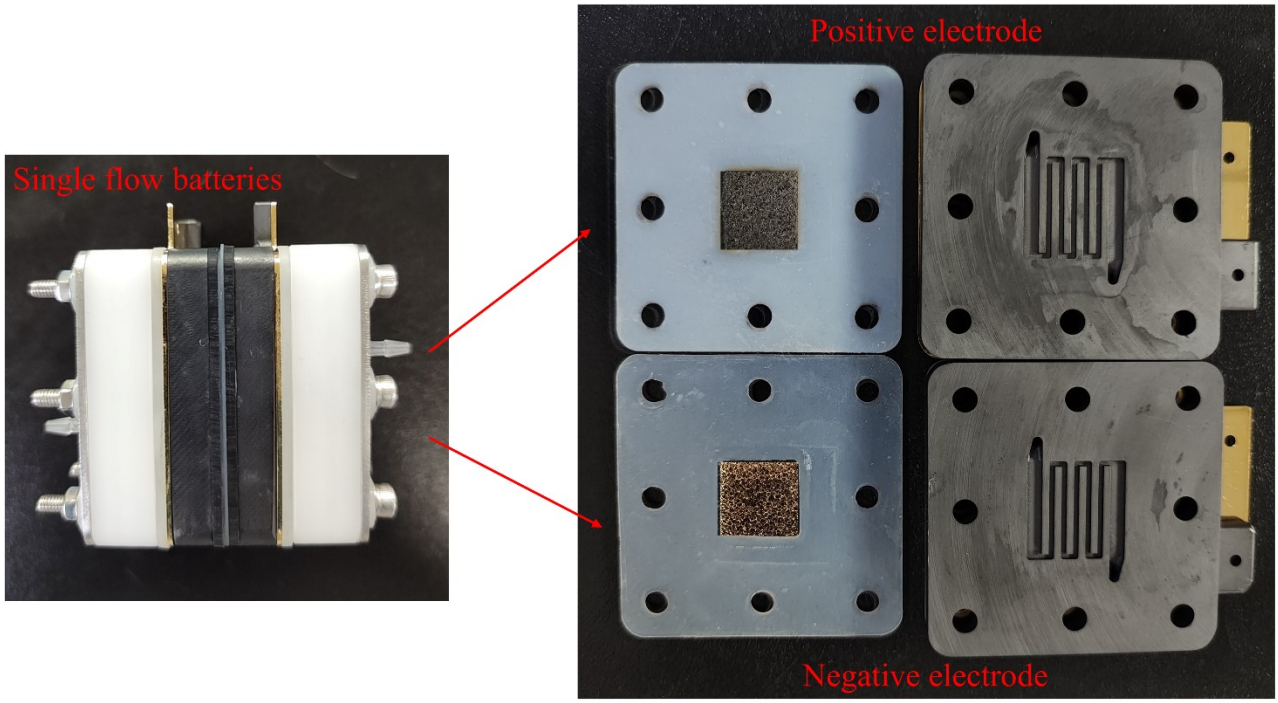

Fig. S3 Schematic diagram of the flow batteries.

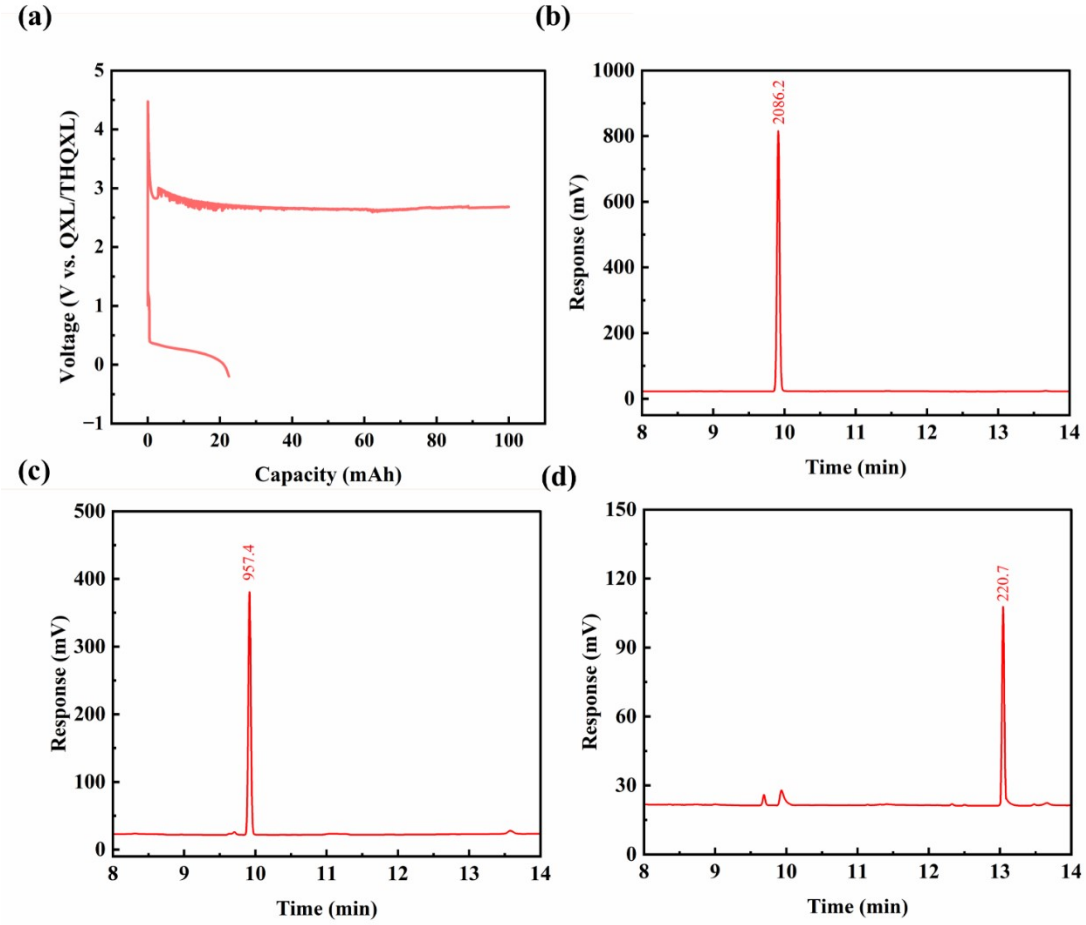

Fig. S4 (a) GCD profile of 0.01 M QXL||$K_4[Fe(CN)_6]$ batteries in ECS9; charging was performed at a current density of 40 mA cm^{-2} to a capacity of 100 mAh. GC analysis of the 0.01 M QXL solution (b) before cycling and (c) after 1 cycle. (d) GC analysis of the ethanol solution after ultrasonic treatment of $CoMoO_4$/NF cycled once.

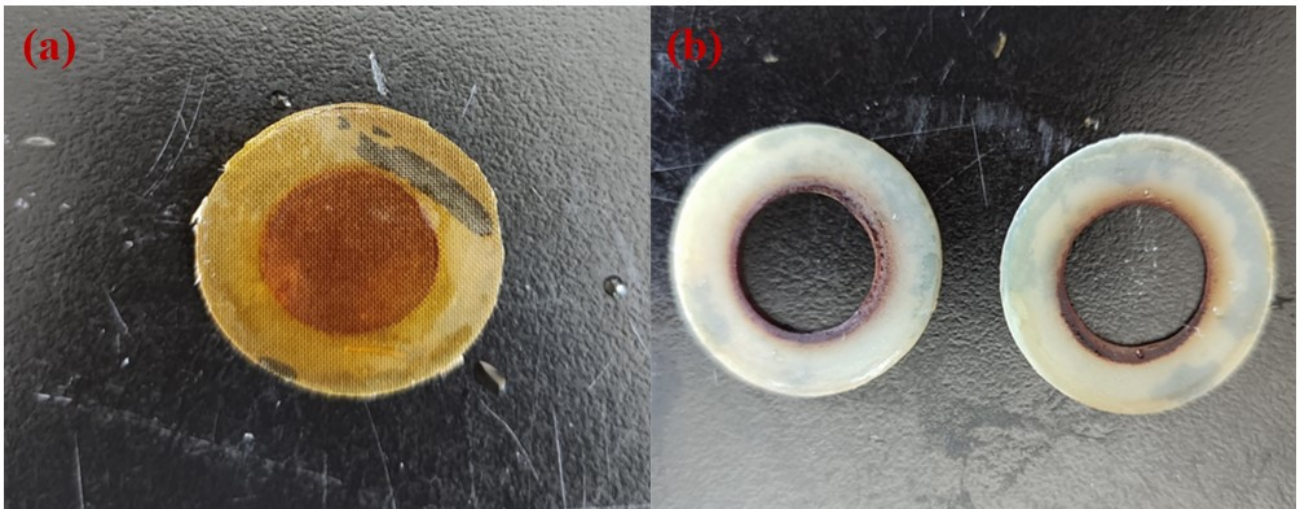

Fig. S5 State of the (a) membrane and (b) gasket in the H-type batteries after 1 cycle.

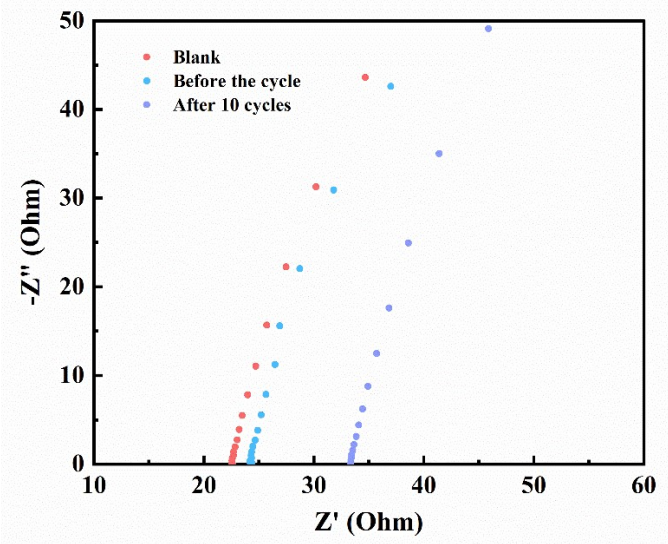

Fig. S6 Nyquist plots of $CoMoO_4$/NF as the working electrode in 0.01 M QXL||$K_4[Fe(CN)_6]$ batteries with ECS9 as a blank control without an ion-exchange membrane and with an ion-exchange membrane before and after 10 cycles.

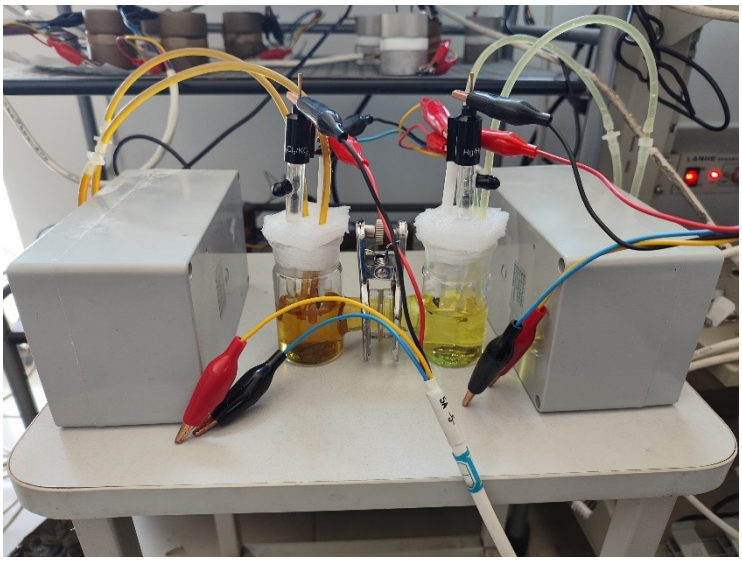

Fig. S7 Three-electrode H-type battery experimental device with electrolyte driven by a peristaltic pump.

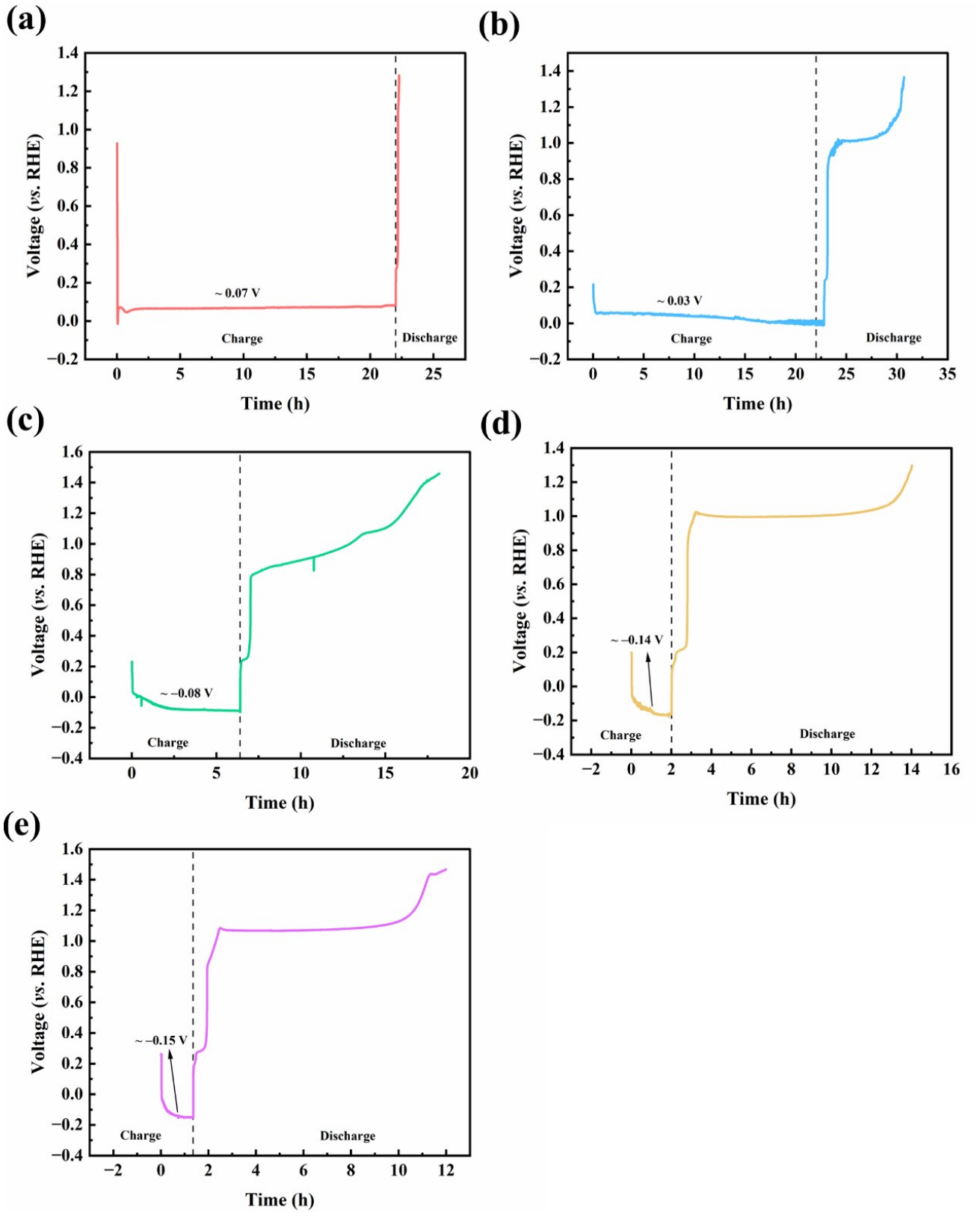

Fig. S8 Voltage curves of $CoMoO_4$/NF as the negative electrode in 0.01 M QXL||$K_4[Fe(CN)_6]$ H-type batteries with ECS9; the charging current densities were (a) 2, (b) 5, (c) 20, (d) 40 and (e) 60 mA cm^{-2}.

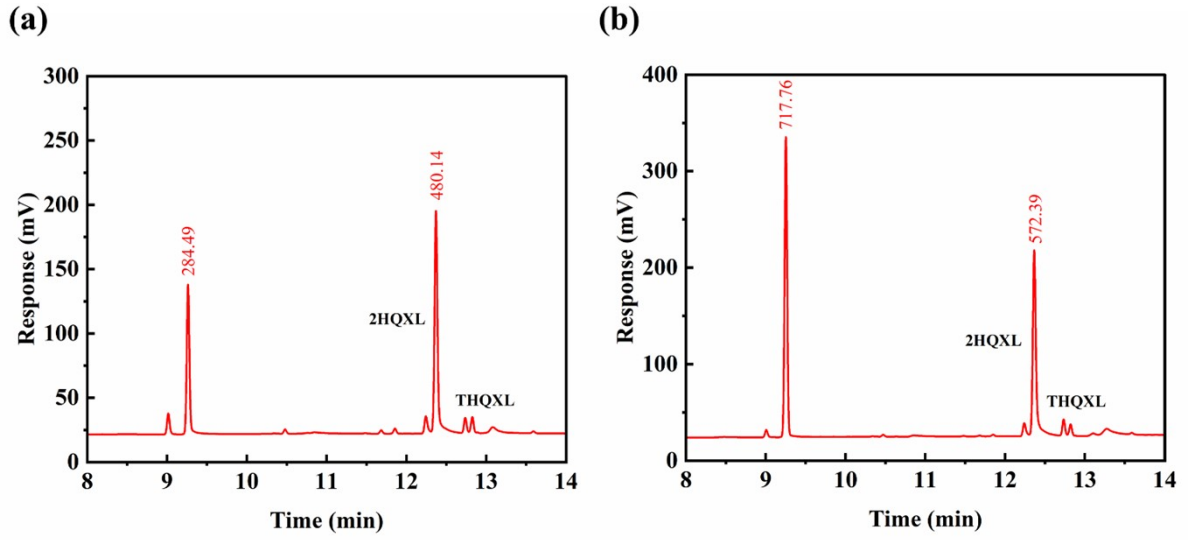

Fig. S9 GC analysis of 0.01 M QXL||$K_4[Fe(CN)_6]$ batteries with ECS8. The batteries were charged at 5 mA cm^{-2} to 80 mAh and then discharged at 2 mA cm^{-2} to –0.2 V. (a) After charging to 80 mAh and (b) after first charging to 80 mAh and then discharging to –0.2 V.

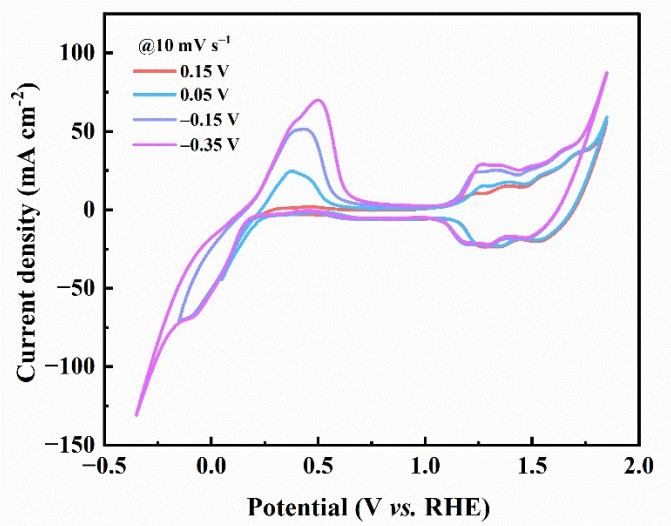

Fig. S10 CV curves of $CoMoO_4$/NF in ECS2 at different potential windows.

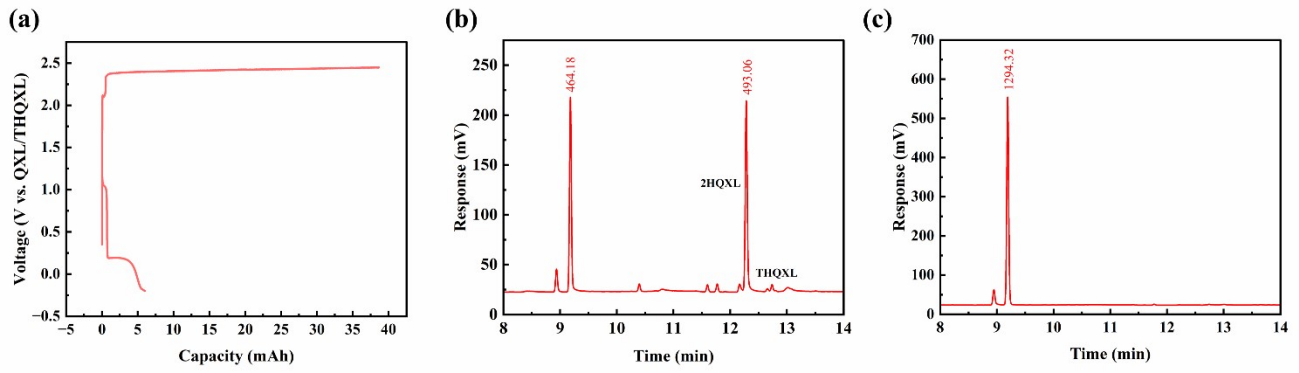

Fig. S11 (a) GCD test for GF in the QXL||$K_4[Fe(CN)_6]$ battery system with ECS11; the charging current density was 20 mA cm^{-2}, and the discharging current density was 2 mA cm^{-2}. GC test (b) after charging to 40 mAh and (c) after first charging to 40 mAh and then discharging to –0.2 V.

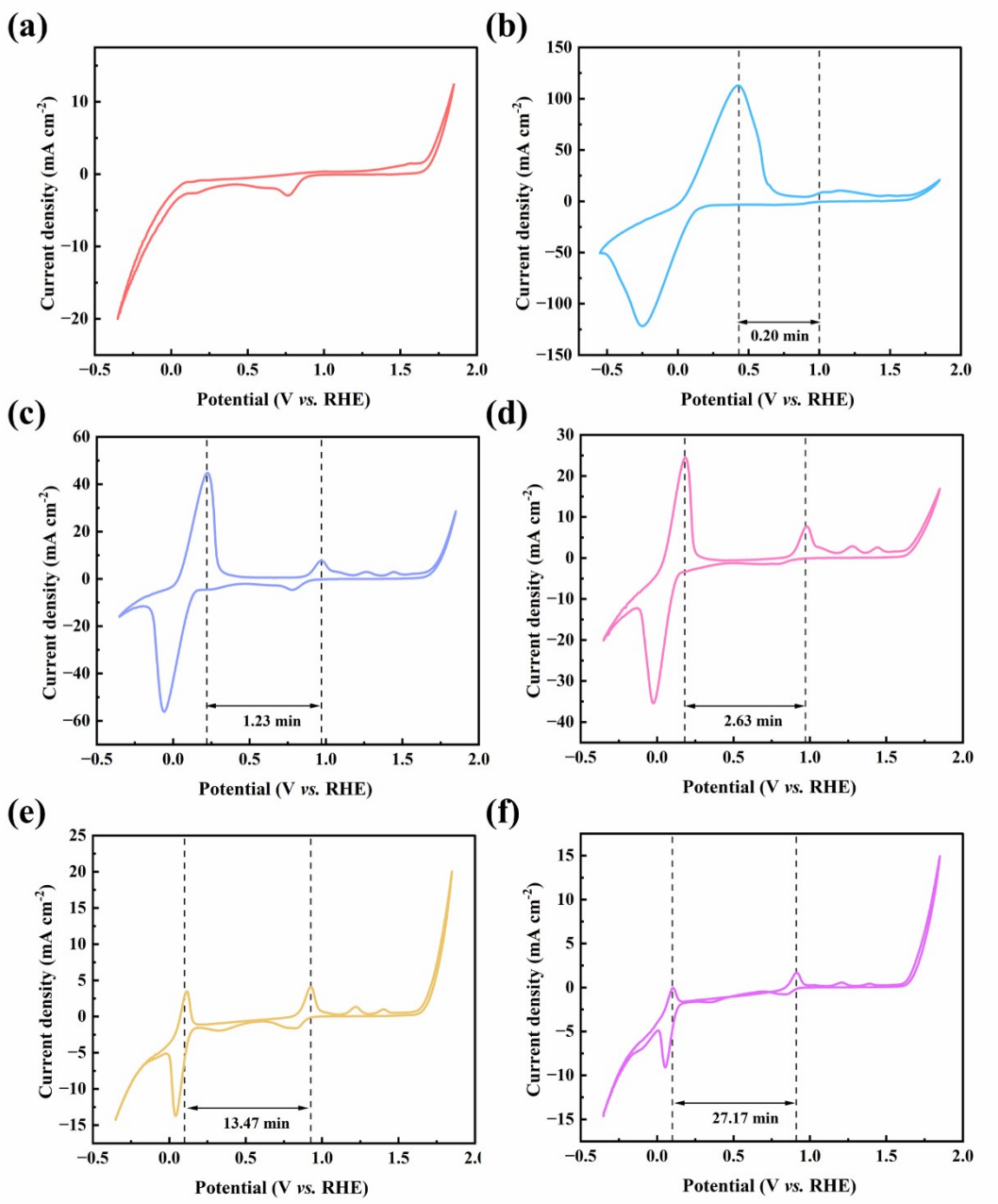

Fig. S12 (a) CV curves of GF in 1 M KOH within ECS12. CV curves at (b) 50, (c) 10, (d) 5, (e) 1 and (f) 0.5 mV s^{-1} for GF in 0.01 M QXL + 1 M KOH.

Table S3 Electrochemical performance of other organic molecule in alkaline aqueous redox flow batteries reported.

Active substances	Molar mass (g/mol)	Electronic number of reactions	Theoretical capacity density (mAh g^{-1})	Concentration of active substances in electrolyte (M)	Cycle number	Ref.
QXL	**130.1**	**4**	**823.7**	**0.01**	**10**	**This work**
2,6-DHAQ	240.2	2	223.1	0.5	100	[1]
DHBQ	140.1	2	382.6	0.5	150	[2]
1,8-PFP	324.4	2	165.2	1.0	53 days	[3]
6-QCA	174.1	2	369.4	0.2	100	[4]
DBEP	384.4	2	139.4	0.6	1024	[5]
2,3-HCNQ	218.2	2	245.7	0.5	100	[6]
BHPC	290.1	2	184.8	0.1	1000	[7]

References

[1] K. Lin, Q. Chen, M.R. Gerhardt, L. Tong, S.B. Kim, L. Eisenach, A.W. Valle, D. Hardee, R.G. Gordon, M.J. Aziz, M.P. Marshak, Alkaline quinone flow battery, *Science*, 2015, 349, 1529–1532. https://doi.org/10.1126/science.aab3033

[2] Z. Yang, L. Tong, D.P. Tabor, E.S. Beh, M.A. Goulet, D. De Porcellinis, A. Aspuru-Guzik, R.G. Gordon, M.J. Aziz, Alkaline benzoquinone aqueous flow battery for large-scale storage of electrical energy, *Advanced Energy Materials*, 2017, 8, 1702056. https://doi.org/10.1002/aenm.201702056

[3] J. Xu, S. Pang, X. Wang, P. Wang, Y. Ji, Ultrastable aqueous phenazine flow batteries with high capacity operated at elevated temperatures, *Joule*, 2021, 42, 185–192. https://doi.org/10.1016/j.joule.2021.06.019

[4] C. Wang, Y. Wang, M. Tao, B. Yu, K. Zhang, J. Wei, Y. Liu, P. Zhang, G. Ding, Z. Tie, J. Cao, Z. Jin, Highly water-soluble 6-quinoxalinecarboxylic acid for high-voltage aqueous organic redox flow batteries, *ACS Applied Energy Materials*, 2022, 5, 10379–10384. https://doi.org/10.1021/acsaem.2c01978

[5] Y. Liu, P. Zhang, Z. Wu, J. Wei, G. Ding, X. Song, J. Ma, W. Wang, Z. Jin, Screening wltra-stable (phenazine)dioxyalkanocic acids with varied water-solubilizing chain lengths for high-capacity aqueous redox flow batteries, *Journal of the American Chemical Society*, 2024, 146, 3293–3302. https://doi.org/10.1021/jacs.3c11887

[6] C. Wang, Z. Yang, Y. Wang, P. Zhao, W. Yan, G. Zhu, L. Ma, B. Yu, L. Wang, G. Li, J. Liu, Z. Jin, High-performance alkaline organic redox flow batteries based on 2-hydroxy-3-carboxy-1,4-naphthoquinone, *ACS Energy Letters*, 2018, 3, 2404-2409. https://doi.org/10.1021/acsenergylett.8b01296

[7] C. Wang, X. Li, B. Yu, Y. Wang, Z. Yang, H. Wang, H. Lin, J. Ma, G. Li, Z. Jin, Molecular design of fused-ring phenazine derivatives for long-cycling alkaline redox flow batteries, *ACS Energy Letters*, 2020, 5, 411–417. https://doi.org/10.1021/acsenergylett.9b02676